NANO LETTERS

pubs.acs.org/NanoLett Letter

# Spin−Orbit Torque Nano-oscillators by Dipole-Field-Localized Spin Wave Modes

Chi Zhang,* Inhee Lee, Yong Pu, Sergei A. Manuilov, Denis V. Pelekhov, and P. Chris Hammel*

Cite This: *Nano Lett.* 2021, 21, 10208−10214 Read Online

ACCESS | Metrics & More | Article Recommendations | Supporting Information

**ABSTRACT:** We demonstrate a high-quality spin−orbit torque nano-oscillator comprised of spin wave modes confined by the magnetic field by the strongly inhomogeneous dipole field of a nearby micromagnet. This approach enables variable spatial confinement and systematic tuning of magnon spectrum and spectral separations for studying the impact of multimode interactions on auto-oscillations. We find these dipole-field-localized spin wave modes exhibit good characteristic properties as auto-oscillators—narrow line width and large amplitude—while persisting up to room temperature. We find that the line width of the lowest-lying localized mode is approximately proportional to temperature in good agreement with theoretical analysis of the impact of thermal fluctuations. This demonstration of a clean oscillator with tunable properties provides a powerful tool for understanding the fundamental limitations and line width contributions to improve future spin-Hall oscillators.

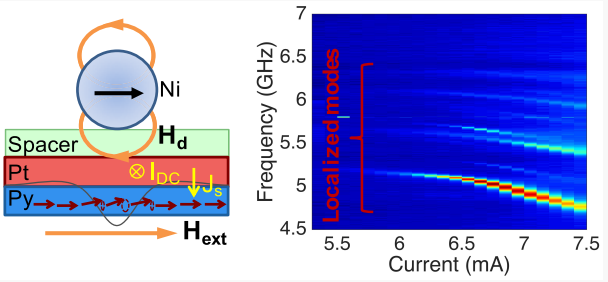


**KEYWORDS:** *spin−orbit torque, spin-Hall nano-oscillators, dipole-field-localized modes, variable spatial confinement*



## INTRODUCTION

The spin-Hall effect (SHE) spin torque can drive magnetic auto-oscillations or excite propagating spin waves[1−5] in a ferromagnet,[6−8] potentially enabling a dc current-tunable microwave source,[9,10] neuromorphic computing,[11,12] and spin−orbit torque magnonics.[1−5] However, nonlinear magnon scattering can degrade the quality of spin-Hall oscillators broadening line width and hampering the achievement of auto-oscillation.[8,13,14] A ferromagnetic film with spatially extended dimensions harbors a large number of degenerate spin wave modes which can enable nonlinear magnon scattering that redistributes energy between modes, hampering coherent oscillation of a desired mode.[13,15,16] These adverse effects can be reduced either by avoiding the degeneracy,[6,17] *e.g., via* spatial localization or by suppressing the nonlinear mode coupling.[4,18] Spatial localization in, *e.g.*, nanoconstrictions and planar nanogap contacts[6,19−29] produces discrete modes whose frequencies lie below the spin wave dispersion for the extended sample thus reducing scattering channels[5,6,13] and enabling auto-oscillation. Alternative to geometrical confinement, a localized region of reduced internal magnetic field generated by the dipole field of a nearby micromagnetic particle confines the spin wave modes in a nanoscale magnetic field well[30−33] thus enabling auto-oscillation. Dipole-field-localized modes offer advantages as spin-Hall oscillators:[33] First, in contrast to most geometrically confined oscillator modes, our field confinement offers *in situ* tunability. In particular, the lateral confinement and field well depth are tunable by particle parameters—size, moment, particle-sample separation—the last of which can be altered *in-operando* and is continuously controllable if the particle is mounted on a cantilever whose height is variable. This provides an *in situ* tunability of the magnon spectrum and mode separations, and hence tuning of nonlinear magnon scattering to control performance of the oscillators. Second, these dipole-field-localized modes are confined by a magnetic field rather than by sample boundaries, thus avoiding artifacts from fabrication imperfection, so they can provide cleaner confinement.

Here, we demonstrate spin-Hall auto-oscillations of localized spin wave modes spatially confined by the magnetic dipole field of a nearby Ni particle above a Py/Pt stripe. Multiple well-resolved localized modes are driven into narrow-line width, large-amplitude auto-oscillations persistent up to room temperature (RT). The auto-oscillating localized modes exhibit a minimum line width of 5 MHz at 80 K which increases to 18 MHz at RT. We observe a line width for the first localized mode that is approximately proportional to temperature and primarily limited by thermal fluctuations. This high-quality oscillator with its *in-operando* tunability of spatial confinement provides a powerful tool for systematic study of the fundamental aspects of spin-Hall oscillators, including the

**Received:** August 10, 2021
**Revised:** November 20, 2021
**Published:** December 6, 2021

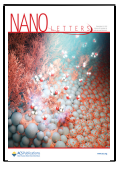

impact of multimode interactions, for advancing the future oscillators.

## METHODS

Py (5 nm)/Pt (5 nm) films are deposited on an undoped-Si substrate by e-beam evaporation. The Py/Pt strips are defined with e-beam lithography using Cr as a hard mask[34] for ion milling. A Ti/Ag/Au coplanar stripline (CPS) is fabricated on the Py/Pt strip *via* photolithography. Figure 1(a) shows a scanning electron micrograph of our device. Three $\mu$m-width strips provide tapered transitions to the 700 nm × 1 $\mu$m region of interest in the center where current density is much higher. This geometry reduces heating and contact resistance. A 150 nm thick $Al_2O_3$ spacer deposited on the device defines its separation from a 1 $\mu$m Ni particle located on top, in the center of the active region, with ±200 nm accuracy in the strip width direction [see the Supporting Information for further details]. We measured two nominally identical devices labeled as Device #1 and Device #2. They show similar results with minimal device-to-device variation [see the Supporting Information]. We report measurements performed at temperatures from 80 K to RT with an external field $H_{ext}$ applied in the film plane at an angle 105° with respect to the orientation of the current flow along the length of the strip. As depicted in Figure 1(b), the spin-Hall effect[35,36] in Pt converts a charge current density $J_C$ into a spin current density $J_S$, which exerts an antidamping spin torque $\tau_{ST}$[37,38] on the Py magnetization. We apply dc charge currents exceeding the critical current needed to fully compensate the damping and excite the auto-oscillation. The microwave power emitted by the device is detected *via* anisotropic magnetoresistance (AMR) effect and measured by a low-noise amplifier and spectrum analyzer.[13,39]

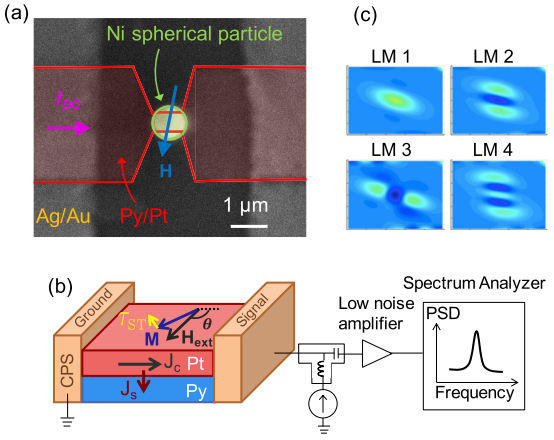


**Figure 1.** (a) Scanning electron micrograph of the Py/Pt strip device (outlined in red) with a Ni spherical particle (outlined in green) glued on top. The active region of the device is the center 700 nm × 1 $\mu$m region of the nanostrip underneath Ni particle. (b) Schematic of auto-oscillation measurement setup. The external field $H_{ext}$ is applied in the plane, at an angle 105° with respect to the direction of the current flow along the length of the strip. The magnetization $M$ and spin torque $\tau_{ST}$ are drawn for the bottom Py layer. (c) Spatial mode profiles of transverse magnetization of the first four lowest-lying localized modes in the 700 nm × 1 $\mu$m active region, labeled as LM1, LM2, LM3, and LM4.

We use a nearby micromagnetic particle to introduce a spatially localized minimum in the internal static field—a field well—in the sample.[30−33] The lowest-frequency spin wave modes at the bottom of the well are discrete localized modes (LM) whose frequencies lie well below the spin wave continuum. In addition, a large number of spin wave modes, both sample-confined modes and highest-order localized modes with high mode densities, reside at the top of the field-well at much higher frequencies. The depth of the field-well, typically several hundreds of Gauss, determines the spectral separation between lowest-lying localized modes and the high-density higher-frequency modes. The spatial confinement provided by the field-well determines the spectral separations between the various discrete localized modes. The four lowest-frequency localized modes are localized width modes LM1 ($n$ = 1, $m$ = 1), LM2 ($n$ = 2, $m$ = 1), a localized length mode LM3 ($n$ = 1, $m$ = 2), and a localized width mode LM4 ($n$ = 3, $m$ = 1).[33] Figure 1(c) shows micromagnetic simulated mode profiles of the lowest-four localized modes in the 700 nm × 1 $\mu$m active region. The mode area of LM1 is about 350 nm × 600 nm.

## RESULTS AND DISCUSSION

Figure 2(a) shows an auto-oscillation color map (as a function of bias current) and representative spectra of Device #2 at $H_{ext}$ = 700 G, $T$ = RT. Below 5.4 mA, there is no signal. Above 5.4 mA, we see a group of several auto-oscillatory modes, corresponding to localized modes that are driven into auto-oscillations [see subsequent further analysis]. The measurements here are done at RT, demonstrating that localized modes function well as RT auto-oscillators which distinguishes them from some existing spin-Hall oscillators.[13,21] If we focus on the first, *i.e.*, lowest-frequency, localized mode, the full width at half-maximum (fwhm) line width, fitted on a linear power scale, decreases to a minimum value of 5 MHz at 8.5 mA at 80 K [Figure 2(b)], which is a typical value for good single spin-Hall oscillators,[13,19−22,40−46] and a much lower value can be achieved in mutually synchronized oscillator arrays.[12] And even at RT, a line width of 18 MHz is still a small value, showing that oscillators derived from dipole-field-localized modes are highly coherent. The signal amplitude initially increases with current. The maximum power of the first localized mode is 0.27 pW at RT and is 2.5 pW at 80 K [see Figure 3(c) or 4(a)], comparable to the 4.6 pW signal size of the bulk mode ($H_{ext}$ = 700 G, $T$ = 80 K) in a bare 700 nm × 1 $\mu$m Py/Pt strip device without a particle. This observation of pW signals from localized modes, even though the signal is only from the reduced local mode area and suffers from current shunting indicates our localized modes are driven into large-amplitude oscillations. The higher-order localized modes become more evident at lower temperatures. A few higher-order localized modes grow into large signals and are as sharp as the first localized mode.

Here, we compare spin torque ferromagnetic resonance (ST-FMR),[48] auto-oscillation and micromagnetic simulation to determine mode nature. Figure 3(a) shows the ST-FMR spectra of Device #1 at 6 GHz with increasing currents. At currents above 2 mA, we see several well-resolved localized modes in the 600−1000 G field range. The localized modes are not individually resolvable below 2 mA (including negative currents), because the line width of the modes, controlled by spin-Hall torque, exceeds or is just comparable to their separation.[33] The signal around 500 G comes from sample-confined modes (SCM) that extend throughout the whole sample but are modified by the field of the particle.[33] Increasing current shifts the resonances of localized modes


https://doi.org/10.1021/acs.nanolett.1c03075
Nano Lett. 2021, 21, 10208−10214

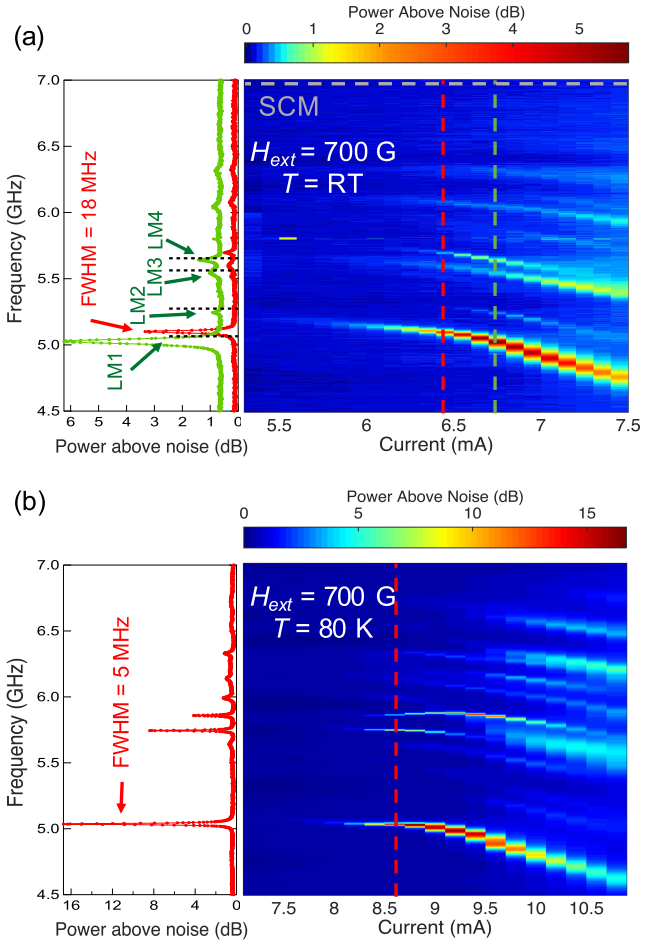


**Figure 2.** Auto-oscillation color maps (as a function of bias current) and representative spectra (corresponding to the vertical dashed line on the color maps) of microwave emission generated by the Py/Pt strip device with a Ni particle (Device #2) at $H_{ext}$ = 700 G, (a) $T$ = RT and (b) $T$ = 80 K. Plotted on the left are the power above noise in units of dB with background subtraction from spectra obtained at 0 mA. In Figure 2(a), the power baseline of the spectrum (green) is manually offset. Black dashed lines in the spectra mark resonance frequencies at 700 G obtained from micromagnetic simulations, enabling identification of the localized modes LM1 to LM4. Dashed horizontal line (gray) in the color map in (a) indicates the frequency of sample-confined modes around 7 GHz extracted from ST-FMR at high current at RT.

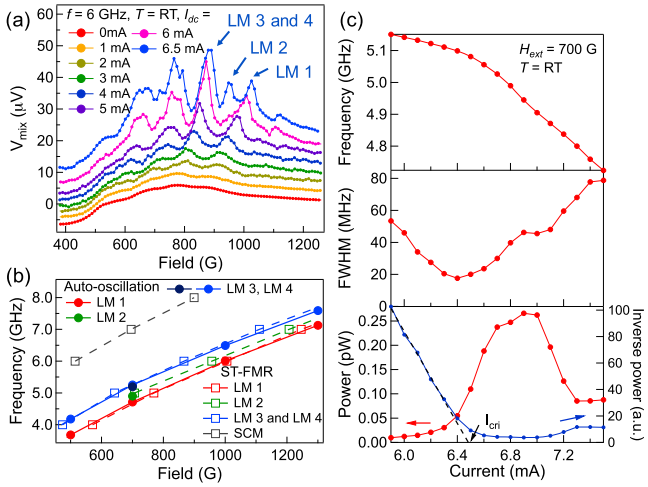


**Figure 3.** (a) ST-FMR spectra of Py/Pt strip device with a Ni particle (Device #1) for several currents at RT and $f$ = 6 GHz. (b) Frequency versus field resonances of LM1 to LM4: (open squares) eigenmodes measured by ST-FMR and (filled circles) auto-oscillatory modes (Device #1). The resonances of sample-confined modes from ST-FMR are shown as a reference. The resonances were extracted at 5.5 mA from ST-FMR and 6.5 mA from auto-oscillation for LM1, 3, and 4. The values for LM2, which appear only at higher currents, were extracted at 6.5 mA from ST-FMR and 6.8 mA from auto-oscillation. (The current values are selected to minimize the nonlinear frequency shift and consider the effect of RF current.) (c) Bias current dependence of the spectral frequency, fwhm line width, integrated power, and inverse integrated power of LM1 auto-oscillation (Device #2). The dashed line in (c) represents a linear fit to inverse power used to identify the critical current.[47]

to higher fields due to Oersted field,[33] Joule heating,[33] and more importantly nonlinear enhancement of the cone angle at high currents.[33,49] We compare resonances of several of the lowest-lying localized modes from ST-FMR and auto-oscillation measurements [see the Supporting Information for auto-oscillation color maps of Device #1] to confirm the nature of the auto-oscillatory modes. The frequency versus field dispersion from both measurements coincide with each other [Figure 3(b)], which confirms that the auto-oscillatory modes arise directly from the localized modes that are confined by the particle field. Then, we perform micromagnetic modeling[30,33,50−52] at $H_{ext}$ = 700 G and compare the resonances with auto-oscillation peaks in Figure 2(a). The simulated resonance frequencies for LM1 to LM4 are shown as dashed lines in Figure 2(a), identifying the first four localized modes [see the Supporting Information for mode identification at other temperatures]. The parameters used in the simulation are $4\pi M_{eff}$ = 8.9 kG, determined from the *in situ* Py/Pt film, the effective magnetization of the unsaturated Ni particle $4\pi M_{Ni}$ = 2400 G which is a free parameter,[31,33] and the modeling is done at $I_{dc}$ = 0. The corresponding localized modes are also labeled in ST-FMR spectra [Figure 3(a)]. We note that the energies of LM3 and LM4 are close, so that their peaks are not distinguishable in ST-FMR. Mode LM2 appears at high currents in ST-FMR and does not present a strong auto-oscillation signal. This could be because the spatial 180° phase reversal in the transverse magnetization of $n$ = 2 mode profile causes partial cancellation in some of the AMR signals.[53] Further details about the observed localized modes in auto-oscillation spectra can be complicated. For LM1−4, we observe all four modes at 700 G, and only observe LM1 and one of the LM3,4 peaks at several other fields [see the Supporting Information for color maps at different fields].

We comment on the modes excited in auto-oscillations. Only the localized modes and second harmonics of the localized modes [see the Supporting Information for full spectrum] are observed. We observe no auto-oscillation signals at the frequencies corresponding to sample-confined modes, while there are signals around those resonance conditions in ST-FMR spectra. This is probably a consequence of the large degeneracies of the modes in this frequency range, both the sample-confined modes and highest-order localized modes.

To systematically study the evolution of the auto-oscillation with current, we subtract a background obtained from the spectrum at 0 mA on a linear scale. We then determine the characteristic parameters of LM1 at $H_{ext}$ = 700 G, $T$ = RT (Device #2) and plot them as a function of current, as shown in Figure 3(c). The current-evolution trends that we observed


https://doi.org/10.1021/acs.nanolett.1c03075
Nano Lett. 2021, 21, 10208−10214

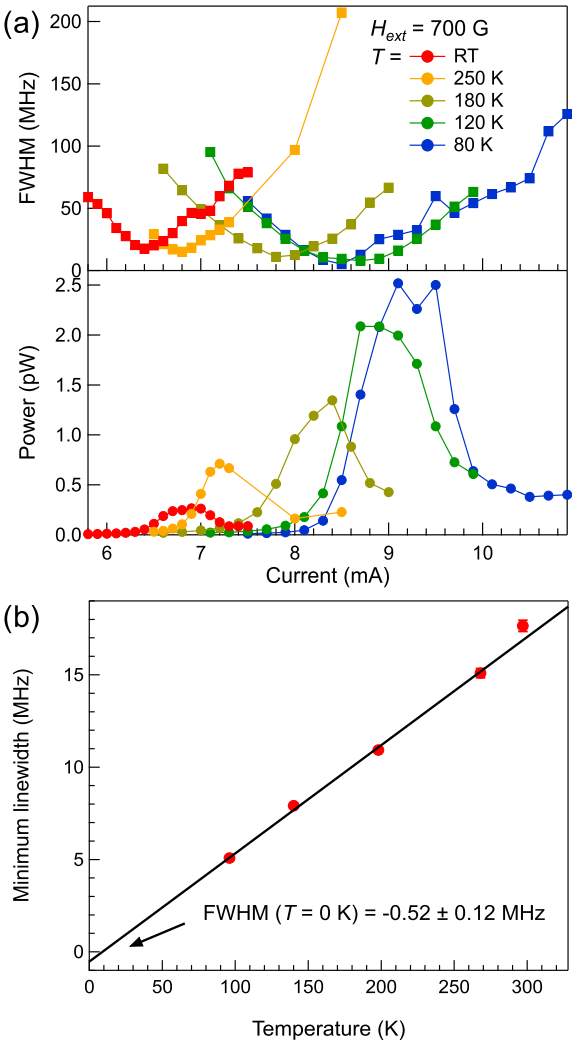


**Figure 4.** Linear temperature dependence of line width (Device #2). (a) Bias current dependence of the fwhm line width and integrated power of LM1 auto-oscillation at different bath temperatures. (b) Actual temperature $T_a$ dependence of the minimum fwhm line width of LM1 auto-oscillation. The error bars in (b) are smaller than the data point.

are similar to ones in existing spin-Hall oscillators.[13,21] A critical current $I_{cri}$ is defined as that at which damping is fully compensated by the spin torque. We extract the critical current $I_{cri}$ *via* a linear fit of inverse power *vs* current.[47] Microwave emission signals can be observed even before the $I_{cri}$, due to thermal fluctuations.[49] Above the critical current, the magnetization precession enters the nonlinear regime as its cone angle increases. In the nonlinear regime, the frequency $\omega$ is a function of the power $p$: $\omega \approx \omega_0 + Np$,[49] where $\omega_0$ is the frequency in small-angle approximation. $N$ is the nonlinear frequency shift coefficient and is typically negative for in-plane field geometries. With increasing current, the power increases leading the frequency to shift to lower values. The shift is slow below $I_{cri}$, because the power is small from thermally excited precessions, becoming rapid above $I_{cri}$ as a consequence of the much larger auto-oscillation power. Below $I_{cri}$, it is in the linear regime, so the line width is linearly reduced by the antidamping torque. If we only consider the nonlinear auto-oscillation theory of a single mode as in conventional spin torque oscillators,[49] the line width would be expected to remain small after the linear reduction. However, here at high currents, the line width broadens and the power drops, which is experimentally observed in other spin-Hall oscillators[13,21] and could be due to nonlinear magnon scattering through the remaining scattering channels.[13]

We further measure current evolution of auto-oscillations at $H_{ext}$ = 700 G at different temperatures (Device #2). The mode structures are qualitatively the same as the ones in Figure 2 [see the Supporting Information]. Figure 4(a) shows the extracted fwhm line width and integrated power of the first localized mode as a function of current for different temperatures. As temperature increases, the required bias current decreases, likely due to an increased spin current conversion efficiency by SHE.[21] The maximum power decreases with increasing temperature, which is generally observed in other spin-Hall oscillators.[13,21]

To determine the temperature dependence of the oscillation line width, we exploit the calibrated dependence of the device's resistance on temperature. This gives the actual temperature $T_a$ of the device in the presence of inevitable Joule heating above the bath temperature $T_b$ by high drive currents which is obtained by measuring the resistance of device[21] [see the Supporting Information]. We analyze the behaviors at the current corresponding to the minimum line width[54,55] as a function of the actual temperature at $H_{ext}$ = 700 G. Figure 4(b) shows that the line width of the first localized mode varies linearly with temperature. The damping has been fully compensated, but the line width of auto-oscillators is a measure of the coherence of the system and the precession periodicity.[39,56] At finite temperatures, thermal fluctuations deflect the magnetization transverse to (amplitude fluctuations) and along (phase fluctuations) its precession trajectory and leads to a spread of the frequencies.[49,57] The generated line width due to thermal fluctuations is expected to be proportional to the temperature.[49] Such a theory accounts well for our data and indicates that the line width of our localized mode oscillator is limited dominantly by thermal fluctuations. A linear fit to the line width data yields an intercept of −0.52 ± 0.12 MHz, close to zero. We compare the temperature dependence of our observed line width with existing auto-oscillators. Ours is the only report of a linear temperature dependence of line width among spin-Hall based oscillators[13,19−22,40−42] with one exception.[54] Even among conventional spin torque oscillators, most temperature dependence studies present unexpected behaviors, more complex than proportional, indicating the existence of other broadening effects.[58−61] Existing reports[55,62,63] of linear temperature dependencies exhibit large negative or positive intercepts. The nonzero intercept is attributed to an additional temperature-independent broadening mechanism,[55,62,63] possibly due to inhomogeneities. Our intercept (both its magnitude and as a percentage of total line width) is the smallest among all these results which may reflect the avoided fabrication-induced broadening afforded by magnetic confinement. We note that the influence of edge damage can be studied by moving the field well toward the edge of the sample to observe the impact of the edge on oscillator performance. Our method of scannable magnetic confinement provides a new approach to understanding problems like these and examining the hypotheses. Additionally, our line width, approximately proportional to temperature, agrees well with Slavin's thermal fluctuations theory. These results suggest our dipole-field-confined oscillator closely approaches a nearly ideal oscillator.


https://doi.org/10.1021/acs.nanolett.1c03075
Nano Lett. 2021, 21, 10208−10214

Beyond fabrication edge imperfections, thermally activated mode hopping[21] (causing exponential temperature dependence) and nonlinear magnon scattering[13,15] can contribute to the line width; field localization of modes is advantageous in relation to these contributions as well. First, localized modes confined by the particle field have large spectral separation from the high density of modes at higher frequencies as well as increased spectral separation between different localized modes and so increase the energy barrier for mode hopping. Second, the tight spatial confinement increases the separation between the discrete lowest-lying localized modes, thus weakening the mechanism of nonlinear magnon scattering.

## CONCLUSIONS

In summary, a new type of spin-Hall oscillator that is spatially confined by a localizing magnetic field is demonstrated. We observe multiple dipole-field-localized spin wave modes driven into auto-oscillation by spin-Hall torque. These localized mode oscillators exhibit good properties: narrow line width, large amplitude, and persistence up to RT. The auto-oscillating localized modes exhibit a line width of 5 MHz at 80 K which increases to 18 MHz at RT. We observe that the line width of the first localized mode is approximately proportional to temperature, limited dominantly by thermal fluctuations. These results indicate a clean oscillator system which provides the opportunity to study auto-oscillators in their intrinsic regime. The concurrence of good properties, proportionality to temperature, and field-localization demonstrates the advantages of field-localization method.

For future applications, the dipole-field localization provides an alternative confining mechanism that can assist further studies and help resolve issues in spin-Hall auto-oscillators, *e.g.*, their spatial self-broadening.[64] In addition, the demonstrated unique strength of localized modes spin-Hall oscillator here can be expanded by putting the particle on a cantilever to scan the localized mode oscillator ($x$ and $y$ directions) and tune well spatial confinement and depth ($z$ direction). We observed signals with a sufficiently strong signal-noise ratio that allows the strip to be widened to a few microns for imaging. Spatial confinement studies tuned by varying cantilever tip−sample separation can reveal the impact of multimode interactions on spin−orbit torque auto-oscillation. Finally, the particle-confined localized modes oscillator combined with spatial-scannability can be utilized to study synchronization[24] and interactions between spatially separated auto-oscillators by varying their lateral separation.

## ASSOCIATED CONTENT

### Supporting Information

The Supporting Information is available free of charge at https://pubs.acs.org/doi/10.1021/acs.nanolett.1c03075.

Comparison of two devices with little device-to-devices variation; auto-oscillation color maps at different fields; full spectrum; actual *vs* bath temperatures; temperature dependence color maps and representative spectra; bare stripe data; Ni particle gluing (PDF)

## AUTHOR INFORMATION


### Corresponding Authors

**Chi Zhang** − *Department of Physics, The Ohio State University, Columbus, Ohio 43210, United States;* orcid.org/0000-0002-2108-8457; Email: zhang.1390@osu.edu

**P. Chris Hammel** − *Department of Physics, The Ohio State University, Columbus, Ohio 43210, United States;* Email: hammel@physics.osu.edu

### Authors

**Inhee Lee** − *Department of Physics, The Ohio State University, Columbus, Ohio 43210, United States*

**Yong Pu** − *Department of Physics, The Ohio State University, Columbus, Ohio 43210, United States;* Present Address: Nanjing University of Posts and Telecommunications, Nanjing 210 023, China

**Sergei A. Manuilov** − *Department of Physics, The Ohio State University, Columbus, Ohio 43210, United States*

**Denis V. Pelekhov** − *Department of Physics, The Ohio State University, Columbus, Ohio 43210, United States*

Complete contact information is available at: https://pubs.acs.org/10.1021/acs.nanolett.1c03075


### Notes

The authors declare no competing financial interest.

## ACKNOWLEDGMENTS

This research was primarily supported by the Center for Emergent Materials, an NSF MRSEC, under award number DMR-2011876. This work was supported in part by an allocation of computing time from the Ohio Supercomputer Center. We also acknowledge technical support and assistance provided by the NanoSystems Laboratory at The Ohio State University partially supported by DMR-2011876.

## REFERENCES


(1) Divinskiy, B.; Demidov, V. E.; Urazhdin, S.; Freeman, R.; Rinkevich, A. B.; Demokritov, S. O. Excitation and Amplification of Spin Waves by Spin-Orbit Torque. *Adv. Mater.* **2018**, *30*, 1802837.

(2) Fulara, H.; Zahedinejad, M.; Khymyn, R.; Awad, A. A.; Muralidhar, S.; Dvornik, M.; Åkerman, J. Spin-orbit torque-driven propagating spin waves. *Science Advances* **2019**, *5*, No. eaax8467.

(3) Demidov, V. E.; Urazhdin, S.; Anane, A.; Cros, V.; Demokritov, S. O. Spin-orbit-torque magnonics. *J. Appl. Phys.* **2020**, *127*, 170901.

(4) Evelt, M.; Soumah, L.; Rinkevich, A.; Demokritov, S.; Anane, A.; Cros, V.; Ben Youssef, J.; de Loubens, G.; Klein, O.; Bortolotti, P.; Demidov, V. Emission of Coherent Propagating Magnons by Insulator-Based Spin-Orbit-Torque Oscillators. *Phys. Rev. Appl.* **2018**, *10*, 041002.

(5) Fulara, H.; Zahedinejad, M.; Khymyn, R.; Dvornik, M.; Fukami, S.; Kanai, S.; Ohno, H.; Åkerman, J. Giant voltage-controlled modulation of spin Hall nano-oscillator damping. *Nat. Commun.* **2020**, *11*, 4006.

(6) Demidov, V. E.; Urazhdin, S.; Ulrichs, H.; Tiberkevich, V.; Slavin, A.; Baither, D.; Schmitz, G.; Demokritov, S. O. Magnetic nano-oscillator driven by pure spin current. *Nat. Mater.* **2012**, *11*, 1028−1031.

(7) Liu, L.; Pai, C.-F.; Ralph, D. C.; Buhrman, R. A. Magnetic Oscillations Driven by the Spin Hall Effect in 3-Terminal Magnetic Tunnel Junction Devices. *Phys. Rev. Lett.* **2012**, *109*, 186602.

(8) Collet, M.; de Milly, X.; d'Allivy Kelly, O.; Naletov, V. V.; Bernard, R.; Bortolotti, P.; Ben Youssef, J.; Demidov, V. E.; Demokritov, S. O.; Prieto, J. L.; Mu noz, M.; Cros, V.; Anane, A.; de Loubens, G.; Klein, O. Generation of coherent spin-wave modes in yttrium iron garnet microdiscs by spin-orbit torque. *Nat. Commun.* **2016**, *7*, 10377.

(9) Kiselev, S. I.; Sankey, J. C.; Krivorotov, I. N.; Emley, N. C.; Schoelkopf, R. J.; Buhrman, R. A.; Ralph, D. C. Microwave oscillations

of a nanomagnet driven by a spin-polarized current. *Nature* **2003**, *425*, 380−383.
(10) Shao, Q.; et al. Roadmap of Spin-Orbit Torques. *IEEE Trans. Magn.* **2021**, *57*, 800439.
(11) Dieny, B.; et al. Opportunities and challenges for spintronics in the microelectronics industry. *Nature Electronics* **2020**, *3*, 446−459.
(12) Zahedinejad, M.; Awad, A. A.; Muralidhar, S.; Khymyn, R.; Fulara, H.; Mazraati, H.; Dvornik, M.; Åkerman, J. Two-dimensional mutually synchronized spin Hall nano-oscillator arrays for neuromorphic computing. *Nat. Nanotechnol.* **2020**, *15*, 47−52.
(13) Duan, Z.; Smith, A.; Yang, L.; Youngblood, B.; Lindner, J.; Demidov, V. E.; Demokritov, S. O.; Krivorotov, I. N. Nanowire spin torque oscillator driven by spin orbit torques. *Nat. Commun.* **2014**, *5*, 5616.
(14) Barsukov, I.; Lee, H. K.; Jara, A. A.; Chen, Y.-J.; Gonçalves, A. M.; Sha, C.; Katine, J. A.; Arias, R. E.; Ivanov, B. A.; Krivorotov, I. N. Giant nonlinear damping in nanoscale ferromagnets. *Science Advances* **2019**, *5*, No. eaav6943.
(15) Demidov, V. E.; Urazhdin, S.; Edwards, E. R. J.; Stiles, M. D.; McMichael, R. D.; Demokritov, S. O. Control of Magnetic Fluctuations by Spin Current. *Phys. Rev. Lett.* **2011**, *107*, 107204.
(16) Demidov, V.; Urazhdin, S.; de Loubens, G.; Klein, O.; Cros, V.; Anane, A.; Demokritov, S. Magnetization oscillations and waves driven by pure spin currents. *Phys. Rep.* **2017**, *673*, 1−31.
(17) Divinskiy, B.; Demidov, V. E.; Kozhanov, A.; Rinkevich, A. B.; Demokritov, S. O.; Urazhdin, S. Nanoconstriction spin-Hall oscillator with perpendicular magnetic anisotropy. *Appl. Phys. Lett.* **2017**, *111*, 032405.
(18) Divinskiy, B.; Urazhdin, S.; Demokritov, S. O.; Demidov, V. E. Controlled nonlinear magnetic damping in spin-Hall nano-devices. *Nat. Commun.* **2019**, *10*, 5211.
(19) Demidov, V. E.; Urazhdin, S.; Zholud, A.; Sadovnikov, A. V.; Demokritov, S. O. Nanoconstriction-based spin-Hall nano-oscillator. *Appl. Phys. Lett.* **2014**, *105*, 172410.
(20) Demidov, V. E.; Urazhdin, S.; Zholud, A.; Sadovnikov, A. V.; Slavin, A. N.; Demokritov, S. O. Spin-current nano-oscillator based on nonlocal spin injection. *Sci. Rep.* **2015**, *5*, 8578.
(21) Liu, R. H.; Lim, W. L.; Urazhdin, S. Spectral Characteristics of the Microwave Emission by the Spin Hall Nano-Oscillator. *Phys. Rev. Lett.* **2013**, *110*, 147601.
(22) Demidov, V. E.; Urazhdin, S.; Divinskiy, B.; Rinkevich, A. B.; Demokritov, S. O. Spectral linewidth of spin-current nano-oscillators driven by nonlocal spin injection. *Appl. Phys. Lett.* **2015**, *107*, 202402.
(23) Haidar, M.; Awad, A. A.; Dvornik, M.; Khymyn, R.; Houshang, A.; Åkerman, J. A single layer spin-orbit torque nano-oscillator. *Nat. Commun.* **2019**, *10*, 2362.
(24) Awad, A. A.; Dürrenfeld, P.; Houshang, A.; Dvornik, M.; Iacocca, E.; Dumas, R. K.; Åkerman, J. Long-range mutual synchronization of spin Hall nano-oscillators. *Nat. Phys.* **2017**, *13*, 292−299.
(25) Sato, N.; Schultheiss, K.; Körber, L.; Puwenberg, N.; Mühl, T.; Awad, A. A.; Arekapudi, S. S. P. K.; Hellwig, O.; Fassbender, J.; Schultheiss, H. Domain Wall Based Spin-Hall Nano-Oscillators. *Phys. Rev. Lett.* **2019**, *123*, 057204.
(26) Hache, T.; Li, Y.; Weinhold, T.; Scheumann, B.; Gonçalves, F. J. T.; Hellwig, O.; Fassbender, J.; Schultheiss, H. Bipolar spin Hall nano-oscillators. *Appl. Phys. Lett.* **2020**, *116*, 192405.
(27) Spicer, T. M.; Keatley, P. S.; Loughran, T. H. J.; Dvornik, M.; Awad, A. A.; Dürrenfeld, P.; Houshang, A.; Ranjbar, M.; Åkerman, J.; Kruglyak, V. V.; Hicken, R. J. Spatial mapping of torques within a spin Hall nano-oscillator. *Phys. Rev. B: Condens. Matter Mater. Phys.* **2018**, *98*, 214438.
(28) Zahedinejad, M.; Mazraati, H.; Fulara, H.; Yue, J.; Jiang, S.; Awad, A. A.; Åkerman, J. CMOS compatible W/CoFeB/MgO spin Hall nano-oscillators with wide frequency tunability. *Appl. Phys. Lett.* **2018**, *112*, 132404.
(29) Dvornik, M.; Awad, A. A.; Åkerman, J. Origin of Magnetization Auto-Oscillations in Constriction-Based Spin Hall Nano-Oscillators. *Phys. Rev. Appl.* **2018**, *9*, 014017.
(30) Adur, R.; Du, C.; Wang, H.; Manuilov, S. A.; Bhallamudi, V. P.; Zhang, C.; Pelekhov, D. V.; Yang, F.; Hammel, P. C. Damping of Confined Modes in a Ferromagnetic Thin Insulating Film: Angular Momentum Transfer across a Nanoscale Field-Defined Interface. *Phys. Rev. Lett.* **2014**, *113*, 176601.
(31) Chia, H.-J.; Guo, F.; Belova, L. M.; McMichael, R. D. Nanoscale Spin Wave Localization Using Ferromagnetic Resonance Force Microscopy. *Phys. Rev. Lett.* **2012**, *108*, 087206.
(32) Lee, I.; Obukhov, Y.; Xiang, G.; Hauser, A.; Yang, F.; Banerjee, P.; Pelekhov, D. V.; Hammel, P. C. Nanoscale scanning probe ferromagnetic resonance imaging using localized modes. *Nature* **2010**, *466*, 845−848.
(33) Zhang, C.; Pu, Y.; Manuilov, S. A.; White, S. P.; Page, M. R.; Blomberg, E. C.; Pelekhov, D. V.; Hammel, P. C. Engineering the Spectrum of Dipole Field-Localized Spin-Wave Modes to Enable Spin-Torque Antidamping. *Phys. Rev. Appl.* **2017**, *7*, 054019.
(34) Duan, Z. Tuning the Damping of Spin Wave Modes by Spin Hall Current in Permalloy/Platinum Wires. *Ph.D. thesis*, University of California, Irvine, 2013.
(35) D'Yakonov, M. I.; Perel', V. I. Possibility of Orienting Electron Spins with Current. *JETP Lett.* **1971**, *13*, 467.
(36) Hirsch, J. E. Spin Hall Effect. *Phys. Rev. Lett.* **1999**, *83*, 1834−1837.
(37) Berger, L. Emission of spin waves by a magnetic multilayer traversed by a current. *Phys. Rev. B: Condens. Matter Mater. Phys.* **1996**, *54*, 9353−9358.
(38) Slonczewski, J. C. Current-driven excitation of magnetic multilayers. *J. Magn. Magn. Mater.* **1996**, *159*, L1−L7.
(39) Thadani, K. Spin-Torque-Driven Microwave Frequency Dynamics In Magnetic Nanopillar Devices. *Ph.D. thesis*, Cornell University, 2009.
(40) Yang, L.; Verba, R.; Tiberkevich, V.; Schneider, T.; Smith, A.; Duan, Z.; Youngblood, B.; Lenz, K.; Lindner, J.; Slavin, A. N.; Krivorotov, I. N. Reduction of phase noise in nanowire spin orbit torque oscillators. *Sci. Rep.* **2015**, *5*, 16942.
(41) Dürrenfeld, P.; Awad, A. A.; Houshang, A.; Dumas, R. K.; Åkerman, J. A 20 nm spin Hall nano-oscillator. *Nanoscale* **2017**, *9*, 1285−1291.
(42) Mazraati, H.; Chung, S.; Houshang, A.; Dvornik, M.; Piazza, L.; Qejvanaj, F.; Jiang, S.; Le, T. Q.; Weissenrieder, J.; Åkerman, J. Low operational current spin Hall nano-oscillators based on NiFe/W bilayers. *Appl. Phys. Lett.* **2016**, *109*, 242402.
(43) Awad, A. A.; Houshang, A.; Zahedinejad, M.; Khymyn, R.; Åkerman, J. Width dependent auto-oscillating properties of constriction based spin Hall nano-oscillators. *Appl. Phys. Lett.* **2020**, *116*, 232401.
(44) Mazraati, H.; Etesami, S. R.; Banuazizi, S. A. H.; Chung, S.; Houshang, A.; Awad, A. A.; Dvornik, M.; Åkerman, J. Auto-oscillating Spin-Wave Modes of Constriction-Based Spin Hall Nano-oscillators in Weak In-Plane Fields. *Phys. Rev. Appl.* **2018**, *10*, 054017.
(45) Chen, L.; Urazhdin, S.; Du, Y.; Liu, R. Dynamical Mode Coupling and Coherence in a Spin Hall Nano-Oscillator with Perpendicular Magnetic Anisotropy. *Phys. Rev. Appl.* **2019**, *11*, 064038.
(46) Chen, L.; Chen, Y.; Zhou, K.; Li, H.; Pu, Y.; Xu, Y.; Du, Y.; Liu, R. Controllable excitation of multiple spin wave bullet modes in a spin Hall nano-oscillator based on[Ni/Co]/Pt multilayers. *Nanoscale* **2021**, *13*, 7838−7843.
(47) Tiberkevich, V.; Slavin, A.; Kim, J.-V. Microwave power generated by a spin-torque oscillator in the presence of noise. *Appl. Phys. Lett.* **2007**, *91*, 192506.
(48) Liu, L.; Moriyama, T.; Ralph, D. C.; Buhrman, R. A. Spin-Torque Ferromagnetic Resonance Induced by the Spin Hall Effect. *Phys. Rev. Lett.* **2011**, *106*, 036601.
(49) Slavin, A.; Tiberkevich, V. Nonlinear Auto-Oscillator Theory of Microwave Generation by Spin-Polarized Current. *IEEE Trans. Magn.* **2009**, *45*, 1875−1918.
(50) Adur, R.; Du, C.; Manuilov, S. A.; Wang, H.; Yang, F.; Pelekhov, D. V.; Hammel, P. C. The magnetic particle in a box:


https://doi.org/10.1021/acs.nanolett.1c03075
*Nano Lett.* 2021, 21, 10208−10214

Analytic and micromagnetic analysis of probe-localized spin wave modes. *J. Appl. Phys.* **2015**, *117*, 17E108.
(51) Du, C.; Adur, R.; Wang, H.; Manuilov, S. A.; Yang, F.; Pelekhov, D. V.; Hammel, P. C. Experimental and numerical understanding of localized spin wave mode behavior in broadly tunable spatially complex magnetic configurations. *Phys. Rev. B: Condens. Matter Mater. Phys.* **2014**, *90*, 214428.
(52) Obukhov, Y.; Pelekhov, D. V.; Kim, J.; Banerjee, P.; Martin, I.; Nazaretski, E.; Movshovich, R.; An, S.; Gramila, T. J.; Batra, S.; Hammel, P. C. Local Ferromagnetic Resonance Imaging with Magnetic Resonance Force Microscopy. *Phys. Rev. Lett.* **2008**, *100*, 197601.
(53) Mecking, N.; Gui, Y. S.; Hu, C.-M. Microwave photovoltage and photoresistance effects in ferromagnetic microstrips. *Phys. Rev. B: Condens. Matter Mater. Phys.* **2007**, *76*, 224430.
(54) Chen, L.; Urazhdin, S.; Zhou, K.; Du, Y.; Liu, R. Magnetic Droplet Mode in a Vertical Nanocontact-Based Spin Hall Nano-Oscillator at Oblique Fields. *Phys. Rev. Appl.* **2020**, *13*, 024034.
(55) Schneider, M. L.; Rippard, W. H.; Pufall, M. R.; Cecil, T.; Silva, T. J.; Russek, S. E. Temperature dependence of spin-torque-driven self-oscillations. *Phys. Rev. B: Condens. Matter Mater. Phys.* **2009**, *80*, 144412.
(56) Sankey, J. Microwave-Frequency Characterization of Spin Transfer and Individual Nanomagnets. *Ph.D. thesis*, Cornell University, 2007.
(57) Chen, T.; Dumas, R. K.; Eklund, A.; Muduli, P. K.; Houshang, A.; Awad, A. A.; Dürrenfeld, P.; Malm, B. G.; Rusu, A.; Åkerman, J. Spin-Torque and Spin-Hall Nano-Oscillators. *Proc. IEEE* **2016**, *104*, 1919−1945.
(58) Muduli, P. K.; Heinonen, O. G.; Åkerman, J. Temperature dependence of linewidth in nanocontact based spin torque oscillators: Effect of multiple oscillatory modes. *Phys. Rev. B: Condens. Matter Mater. Phys.* **2012**, *86*, 174408.
(59) Sankey, J. C.; Krivorotov, I. N.; Kiselev, S. I.; Braganca, P. M.; Emley, N. C.; Buhrman, R. A.; Ralph, D. C. Mechanisms limiting the coherence time of spontaneous magnetic oscillations driven by dc spin-polarized currents. *Phys. Rev. B: Condens. Matter Mater. Phys.* **2005**, *72*, 224427.
(60) Georges, B.; Grollier, J.; Cros, V.; Fert, A.; Fukushima, A.; Kubota, H.; Yakushijin, K.; Yuasa, S.; Ando, K. Origin of the spectral linewidth in nonlinear spin-transfer oscillators based on MgO tunnel junctions. *Phys. Rev. B: Condens. Matter Mater. Phys.* **2009**, *80*, 060404.
(61) Mistral, Q.; Kim, J.-V.; Devolder, T.; Crozat, P.; Chappert, C.; Katine, J. A.; Carey, M. J.; Ito, K. Current-driven microwave oscillations in current perpendicular-to-plane spin-valve nanopillars. *Appl. Phys. Lett.* **2006**, *88*, 192507.
(62) Bortolotti, P.; Dussaux, A.; Grollier, J.; Cros, V.; Fukushima, A.; Kubota, H.; Yakushiji, K.; Yuasa, S.; Ando, K.; Fert, A. Temperature dependence of microwave voltage emission associated to spin-transfer induced vortex oscillation in magnetic tunnel junction. *Appl. Phys. Lett.* **2012**, *100*, 042408.
(63) Sierra, J. F.; Quinsat, M.; Garcia-Sanchez, F.; Ebels, U.; Joumard, I.; Jenkins, A. S.; Dieny, B.; Cyrille, M.-C.; Zeltser, A.; Katine, J. A. Influence of thermal fluctuations on the emission linewidth in MgO-based spin transfer oscillators. *Appl. Phys. Lett.* **2012**, *101*, 062407.
(64) Demidov, V. E.; Evelt, M.; Bessonov, V.; Demokritov, S. O.; Prieto, J. L.; Mu noz, M.; Ben Youssef, J.; Naletov, V. V.; de Loubens, G.; Klein, O.; Collet, M.; Bortolotti, P.; Cros, V.; Anane, A. Direct observation of dynamic modes excited in a magnetic insulator by pure spin current. *Sci. Rep.* **2016**, *6*, 32781.


https://doi.org/10.1021/acs.nanolett.1c03075
*Nano Lett.* 2021, 21, 10208−10214